Supporting Information

Massively Parallel and Highly Quantitative Single-Particle Analysis on Interactions between Nanoparticles on Supported Lipid Bilayer

Young Kwang Lee, Sungi Kim, Jeong-Wook Oh and Jwa-Min Nam*

Department of Chemistry, Seoul National University, Seoul, 151-747, South Korea,
*Correspondence to: jmnam@snu.ac.kr

1. SUPPORTING METHODS

Materials. 1,2-dioleoyl-sn-glycero-3-phosphocholine (DOPC), 1,2-dioleoyl-sn-glycero-3-phosphoethanolamine-N-(cap biotinyl) sodium salt (biotinylated DOPE), 1,2-dioleoyl-sn-glycero-3-phosphoethanolamine-N-[methoxy(polyethylene glycol)-1000] ammonium salt (PEG-DOPE), and 1-oleoyl-2-{6-[(7-nitro-2-1,3-benzoxadiazol-4-yl)amino]hexanoyl}-sn-glycero-3-phosphocholine (NBD-PC) were obtained from Avanti Polar Lipids (Alabaster, AL, USA). Cy3-modified streptavidin (STV) was purchased from Molecular Probes (Eugene, OR, USA). Carboxymethyl Polyethylene glycol (M.W. 5000) was purchased from Laysan Bio Inc. (Arab, AL, USA). Bovine serum albumin (BSA), sodium dodecyl sulfate (SDS) and dithiothreitol (DTT) was purchased from Sigma-Aldrich (St. Louis, MO, USA). Phosphate-buffered saline (PBS) solution (0.15 M) was prepared by dissolving NaH_2PO4, Na_2HPO_4 and NaCl (Sigma-Aldrich, St. Louis, MO, USA) in DI water, yielding 10 mM phosphate-buffered solution with 150 mM NaCl (pH 7.4). 0.025 M PBS was prepared to contain 25 mM of NaCl with the same reagents. Nanopure water with the minimum resistance (>18 MΩ cm^{-1}) was used in all the experiments. For the lipid vesicle preparation (vesicle extrusion),

polycarbonate (PC) filters (Whatman, Fisher Scientific) with a pore diameter of 100 nm were used. Organic solvents such as chloroform, acetone and ethanol were obtained from Duksan Pure Chemicals Co. Ltd. (Kyeongi-do, South Korea). Sulfuric acid and hydrogen peroxide were purchased from Daejung Chemicals & Metals Co. Ltd. (Kyeongi-do, South Korea). 50 nm gold nanoparticles and oligonucleotides were purchased from BBI Life Sciences (Cardiff, UK) and Integrated DNA Technology (Coralville, IA, USA), respectively. The target capture sequence for immobile plasmonic nanoparticle (I-PNP) is 5'-HS-$(CH_2)_6$-PEG_6-CTTTGAGCACATCCTTATCAATATT-3' and the supported lipid bilayer (SLB) tethering sequence for I-PNP is 5'-HS-$(CH_2)_6$-PEG_6-CTTTGAGCACTGTTAGCGTGTGTGGAATTTTAAT-biotin-3'. The target capture sequence for M-PNP is 5'-TAACAATAATCCCTCCACGAGTTTC-PEG_6-$(CH_2)_3$-SH-3' and the SLB tethering sequence for mobile plasmonic nanoparticle (M-PNP) is 5'-biotin-TAATTTTAAGGTGTGTGCGATTGTCACGAGTTTC-PEG_6-$(CH_2)_3$-SH-3'. The target sequence is 5'-GAGGGATTATTGTTAAATATTG*A*TAAG GAT-3'. For single-base-pair-mismatched DNA sequence, A (underlined italic letter) in the target DNA sequence was replaced with T. The noncomplementary DNA sequence is 5'-CTG ATT ACT ATT GCA TCT TCC GTT ACA ACT-3'.

2. SUPPORTING DISCUSSION

2.1. Optical stability test for plasmonic nanoparticle probes

The resonant light scattering of metal nanoparticles has a different physical origin from the fluorescence from organic dyes. The radiative damping of localized surface plasmon creates scattered photons, and this process is free to blinking and photobleaching. Such a

unique light scattering mechanism and chemical stability of AuNPs produce strong and constant optical signals. To evaluate photostability of PNPs, the 50 nm AuNPs on the SLB were continuously exposed to dark-field microscopy illumination for 30 min and the scattering intensity was recorded every 6 sec (Fig. S1). The particles remained shining without change in the intensity over the whole experimental time. This indicates the AuNPs are more robust optical labels for real-time optical study than fluorescence dyes that substantially lose the signals within a few minutes even when multiple dyes are employed for single-particle tracking.[43]
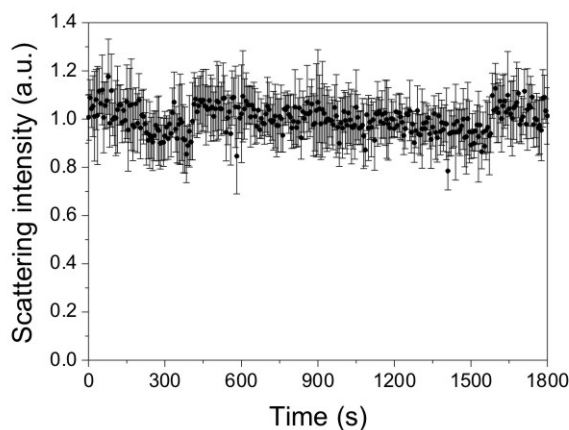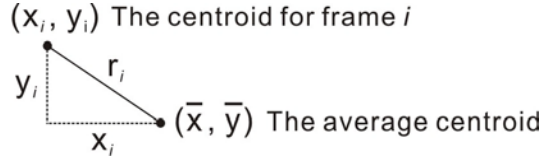

Figure S1. The scattering intensity of the SLB-tethered PNP probes under the continuous dark-field illumination. The optical signal was recorded and calculated every 6 s from 7 individual I-PNP probes.

2.2. Spatial precision of the dark-field microscopy experiment

Spatial precision was calculated from dark-field microscope images of gold nanoparticles immobilized on a glass substrate functionalized with aminopropyltriethoxysilane. For this, a glass substrate was sonicated in chloroform, acetone and water, and followed by piranha

etching (3:1 mixture of H_2SO_4 and H_2O_2). A cleaned substrate was immersed in reaction solution containing 100 mL of methanol, 5 mL of acetic acid and 1 mL of aminopropyltriethoxysilane. After 30 min, a substrate was cleaned with ethanol for three times, and dried with a stream of N_2 gas. Gold nanoparticle solution (2 pM) was placed on a glass surface, and washed with DIW after 1 min. Gold nanoparticles were immobilized on a glass substrate by electrostatic interaction. A droplet of water was dropped on a gold nanoparticle modified glass substrate, and covered by a glass coverslip to carry out dark-field microscopy measurement. Dark-field microscope images were analyzed to determine the centroid of immobilized gold nanoparticles by MOSAIC imageJ plugin software.[43] The spatial precision was defined as the standard deviation of the centroids for 200 frames of data. The standard deviation in two dimensions (σ_{xy}), which determines the spatial precision, was calculated as follows:

(x_i, y_i) The centroid for frame i

$$\sigma_{xy}^2 = \sum_{i=1}^{n} \frac{\left(\sqrt{r_i^2}\right)^2}{N} = \sum_{i=1}^{n} \frac{\left(\sqrt{\left(x_i - \bar{x}\right)^2 + \left(y_i - \bar{y}\right)^2}\right)^2}{N} = \sigma_x^2 + \sigma_y^2 \qquad (1)$$

$$\therefore \sigma_{xy} = \sqrt{\sigma_x^2 + \sigma_y^2} \qquad (2)$$

The spatial precision was determined from equation 2, and found to be 13.81±5.80 nm. It is worth mentioning that spatial precision shown in Table S1 is not related to capability to differentiate nanoparticle interactions. This value provides information on how accurately individual single nanoparticle positions can be measured when they are optically separated under the dark field microscopy. We did not directly measure the distance between two nanoparticles in the dark-field microscope image, because when two particles are interacting

with each other to be assembled, they come close to each other below sub-diffraction length scale and thus are shown as a single objective. However, we can differentiate intimate interactions between nanoparticles below several tens of nanometers based on plasmonic coupling of interacting nanoparticles.

Nanoparticle ID	σ_{X} (nm)	σ_{X} (nm)	σ_{XY} (nm)
1	8.29	6.27	10.39
2	7.64	5.28	9.29
3	9.74	7.17	12.09
4	6.69	4.55	8.09
5	19.38	14.21	24.03
6	9.17	8.11	12.24
7	12.76	10.02	16.22
8	11.26	8.15	13.90
9	20.01	12.24	23.46
10	6.39	5.42	8.38
Average spatial precision			13.81±5.80

Table S1. Result summary of spatial precision of the dark-field microscopy experiment. The ten nanoparticles were analyzed for calculating the average spatial precision and the standard deviation.

2.3. The control and quantification of the biotin valency per gold nanoparticle

We controlled the diffusion of the lipid-tethered plasmonic nanoparticles (PNPs) by changing the biotin valency of PNPs. It was shown that the number of ligands per particle has a significant effect on the lateral mobility of nanoparticles on a lipid membrane.[32,44] We adjusted the valency of the biotin molecules on AuNPs during the DNA functionalization

step by varying the molar ratios between target capture DNA sequence and SLB tethering DNA sequence. This stoichiometric control method yielded highly reproducible results. The number of SLB tethering sequences per PNP was estimated by measuring the fluorescence emission intensity of Cy3 molecules that were modified to SLB tethering sequences after dissolving AuNPs with KCN solution. The average biotin valency increased linearly from ~0.57 to ~128 as increasing the added amount of SLB tethering DNA linker (Fig. S2 and Tab. S2). The prepared PNP probes were tethered to the SLB surface via biotin-streptavidin interactions. The PNP probes on a SLB with a biotin valency of 0.57 were considered that they had 1 biotin because biotin-free PNPs could not bind to the SLB and could be completely washed out from the surface.
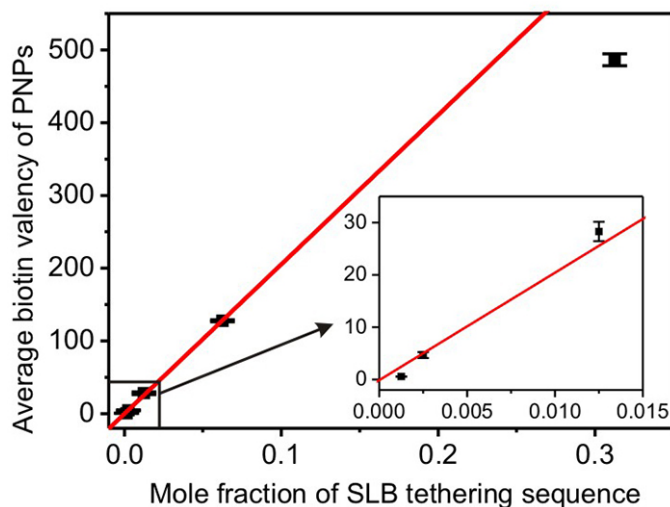
Figure S2. The average number of biotinylated DNA strands on a PNP probe as a function of the mole fraction of the SLB tethering sequence. The values were obtained by averaging independently prepared three different samples. A linear fit was calculated with the experimental values ranging from 0.00125 to 0.0625 ($R^2 = 0.998$).

| Mole fraction of SLB tethering sequence (total concentration: 4μM)	Average biotin valency of PNPs
0.00125	0.569±0.008 (~1 for tethered PNP)
0.0025	4.660±0.564
0.0125	28.297±1.850
0.0625	127.78±1.351
0.3125	486.46±8.008

Table S2. The result summary of the average number of biotinylated DNA strands on a PNP probe with respect to the mole fraction of the SLB tethering sequence.

2.4. The effect of the biotin valency on the diffusive dynamics of PNP probes on a supported lipid bilayer

The lateral motions of SLB-tethered PNP probes were observed with a single nanoparticle resolution using the dark-field microscopy, and their individual trajectories were analyzed by an image analysis program (ImageJ software; please see the methods section in Supporting Information for the experimental details of the single-PNP tracking and analysis process) The mean square displacement (MSD) values as a function of time of the SLB-tethered PNP probes with different biotin valencies are shown in Fig. S3a. Multivalent PNPs showed a tendency to diffuse much more slowly and travel a shorter distance as compared to paucivalent PNPs. The PNP with 486 biotins was nearly immobile and stayed in the almost same position. The MSD plots of these trajectories, except for the 486 biotins case, clearly exhibit the linear relationships between the MSD and time interval, suggesting that these nanoparticles are in a random 2D Brownian motion on the SLB surface. In order to calculate the diffusion coefficients of the PNP probes, we analyzed 100 particle trajectories for each biotin valency and the corresponding MSD plots were fitted to the equation, $<r^2> = 4Dt$, where $<r^2>$ is the MSD, D is the diffusion coefficient, and t is the time interval. The average values of the diffusion coefficients were estimated to be 1.79±0.87 × 10⁻⁸, 0.72±0.35

$\times$ 10^{-8}, 0.38±0.29 $\times$ 10^{-8} and 0.18±0.14 $\times$ 10^{-8} cm^2/s for biotin valency of 1, 5, 28 and 128, respectably (Fig. 2b). The distributions of calculated D values were plotted in Fig. S3b-e and these values are consistent with other literature results where SLBs were modified with 30-50 nm of AuNPs for the visualization of lipid motion.[26,30] As PNPs become more multivalent, the mobile fraction was more reduced, and most particles were virtually immobile when the biotin valency reaches 486. We observed and correlated a dark-field microscope image of multivalent PNPs and a fluorescence microscope image of Cy3-modified streptavidins (STVs) on the SLB to prove the position of PNPs matches with the position of locally concentrated STVs. The results show that two images are well matched to each other, suggesting that local accumulation of STVs under the multivalent PNP is responsible for the loss of particle mobility (Fig. S4).
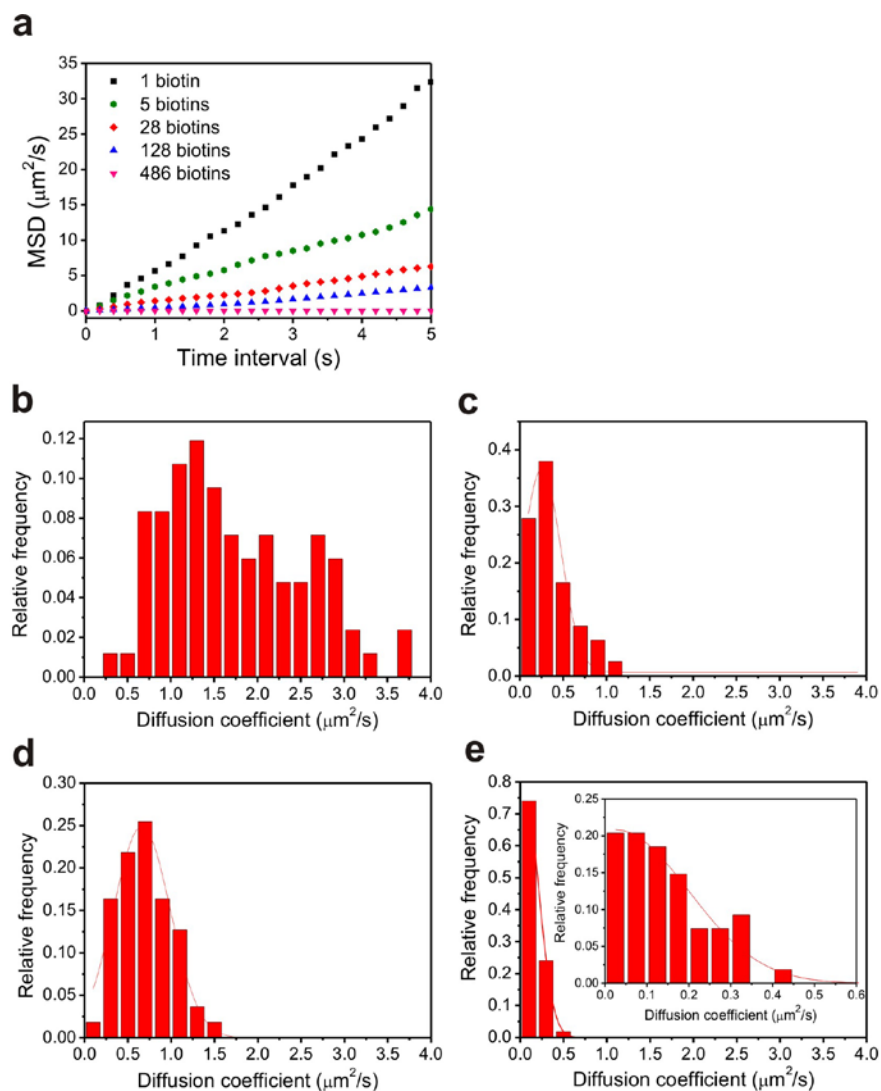
Figure S3. Analysis of diffusion behaviour of gold nanoparticles on a supported lipid bilayer. a, The mean square displacements of the PNPs as a function of time interval. **b-e**, The distributions of diffusion coefficients as changing the biotin valency. The biotin valencies per probe are (b) 1, (c) 5, (d) 25 and (e) 128.
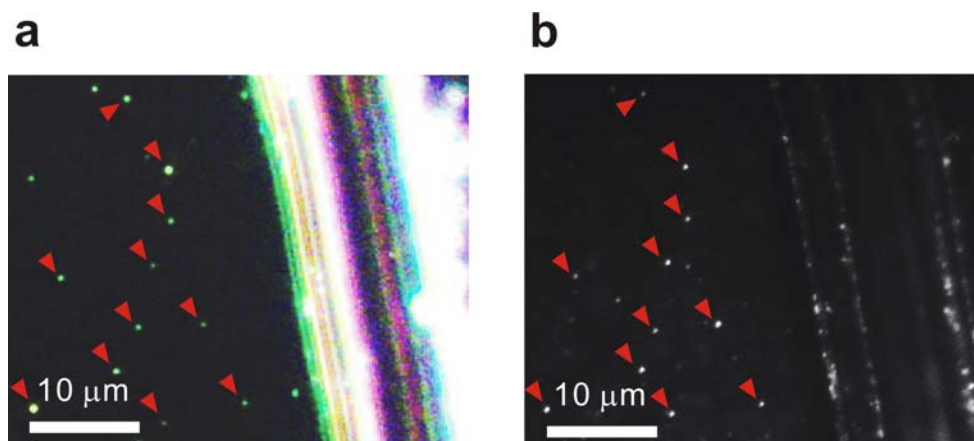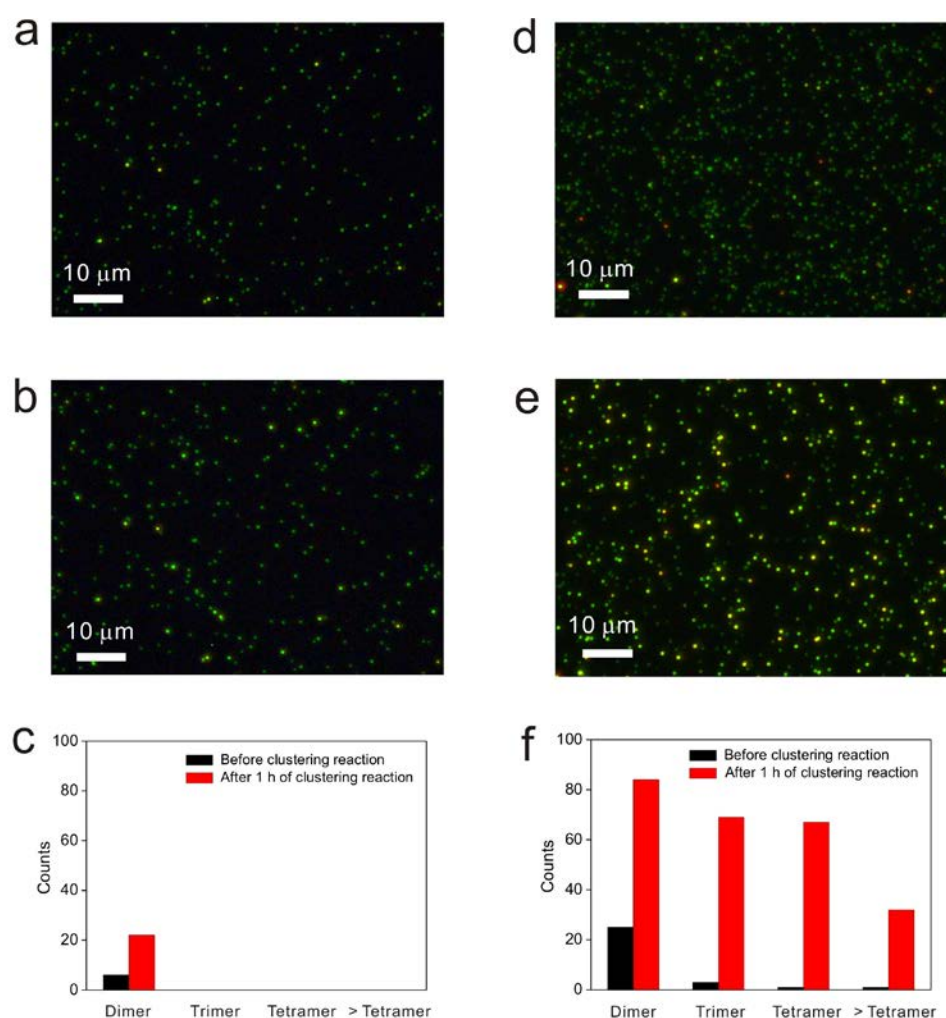
Figure S4. a, The dark-field micorscope image of I-PNP with a biotin valency of 486 on the STV-coated SLB. **b**, The fluorescence microscope image of Cy3-modified STV on the I-PNP-modified SLB. The brightness and contrast of the images were adjusted for clear visualization.

2.5. Comparison of nanoparticle interactions on the lipid bilayer with near the surface.

We found nanoparticle interaction is much more effective when they are tethered to the lipid bilayer. We performed nanoparticle cluster-forming reactions on lipid bilayer and near the surface, and compared the results. For reactions on the lipid bilayer, both mobile (~120 amole nanoparticles/3.7 mm^2) and immobile nanoparticles (~30 amole nanoparticles/3.7 mm^2) were tethered to the lipid bilayer, and clustered by target DNA hybridization. In this case, mobile nanoparticles should two-dimensionally diffuse into immobile nanoparticles for cluster reaction to take place on the lipid bilayer. For reactions near the surface, only immobile probes (~30 amole nanoparticles/3.7 mm^2) were modified on the lipid bilayer and mobile particles (~120 amole nanoparticles/50 µl) were dispersed in bulk solutions. In this case, mobile nanoparticle should diffuse from bulk solution, and react near the surface with immobile particles. The result shows that the nanoparticle clusters are much more efficiently

developed when they are tethered to the lipid bilayer (Fig. S5). I-PNPs on the lipid bilayer were reacted with solution-dispersed M-PNPs, but formed only dimers occasionally. However, we observed much more frequent dimer and multimeric cluster growths in the reactions between I-PNPs and M-PNPs when they both were tethered to the lipid bilayer. The lipid bilayer precaptures gold nanoparticles, and restrict a diffusion mode into the two-dimensional planar surface. The two-dimensional concentration of gold nanoparticles and reduced degree of freedom boost clustering kinetics by increasing both absolute collision frequency and effective collision probability, and providing more proper nanoparticle orientation to be assembled as well.

**Figure S5.** The dark-field microscope image results of **(a, b)** the surface reaction experiment

and (**d, e**) the lipid bilayer reaction experiment. **a**, I-PNP-modified SLB **b**, I-PNP-modified

SLB reacted with M-PNP dispersed in solution for 1 h. Concentration of target DNA

sequence is 300 pM. **c,** Quantitative analysis of nanoparticle cluster formations by the

reactions between I-PNPs on the lipid bilayer and M-PNPs in solution. **d**, I-PNP and M-PNP-

tethered SLB. **e**, I-PNP and M-PNP-tethered SLB reacted with 300 pM of target DNA

sequence for 1 h. **f,** Quantitative analysis of nanoparticle cluster formation by the reactions

between I-PNPs and M-PNPs on the lipid bilayer. The clustering degrees of nanoparticles

were analyzed based on the intensity calibration standard plot in Fig. 4a.

2.6. The coalescence between PNP clusters in the I-PNP-free M-PNP-modified SLB.
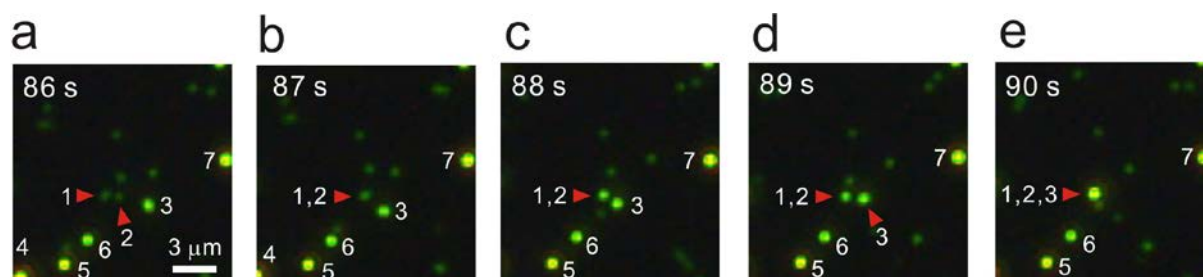
Figure S6. The cluster growth via the combination of monomeric PNP attachment (**a-c**) and

subsequent coalescence between dimeric and trimeric PNP clusters (**d, e**) in an M-PNP pair-

modified SLB without I-PNPs (DNA sequences on M-PNPs can be hybridized to each other

in this case). **a**, Two monomeric PNPs (the red arrows) approaching each other. **b**, The distant

optical overlapping of two PNP monomers. **c**, DNA hybridization-mediated PNP dimer (the

red arrow) formation and consequent plasmonic coupling. **d**, PNP dimer (the left red arrow)

and PNP trimer (the right red arrow) approaching to each other. **e**, The coalescence between

PNP dimer and PNP trimer. The nanoparticles and clusters are marked with numbers for

tracking and identification. The original movie is shown in Supporting Movie S5.

2.7. The scattering intensity distributions as a function of the number of probes per cluster and the average scattering intensity of biotinylated DNA-free PNPs.
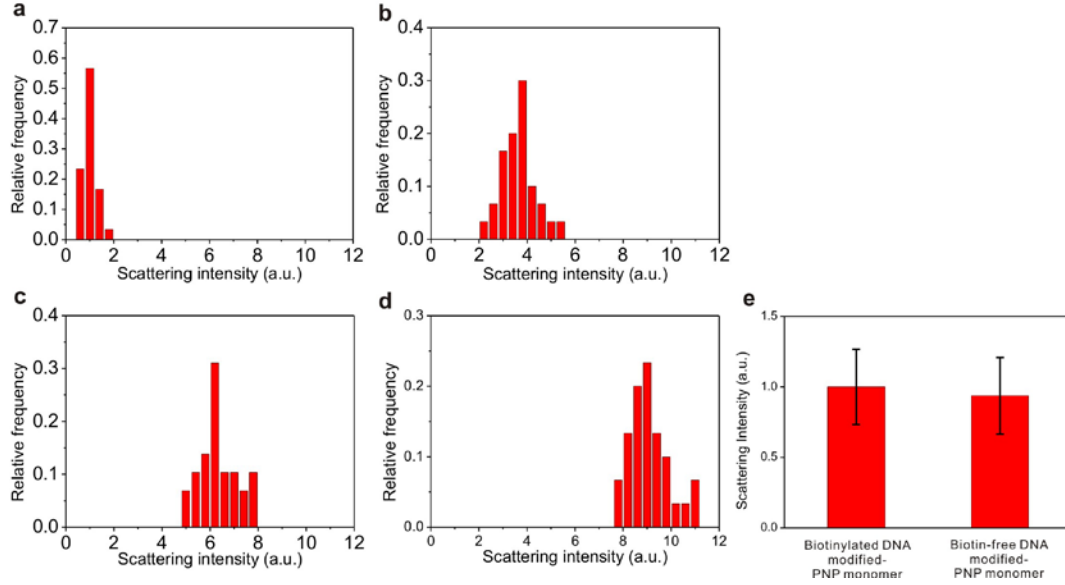
Figure S7. The scattering intensity distributions of PNP clusters as a function of the clustering degree (**a**, Monomer. **b**,Dimer. **c**, Trimer. **d**, Tetramer.; $N = 30$ clusters). **e**, The average scattering intensity of biotinylated DNA-modified PNP monomer and biotin-free DNA-modified PNP monomer.

2.8. The analysis of the cluster growth kinetics

The cluster growth kinetics from monomer to tetramer was fitted to the three-step first-order consecutive reactions by assuming M-PNPs are present in excess compared to I-PNPs:

$$\text{Monomer (M)} \xrightarrow{k_1} \text{Dimer (D)} \xrightarrow{k_2} \text{Trimer (Tr)} \xrightarrow{k_3} \text{Tetramer (Tt).} \qquad (3)$$

The differential forms for the rates of change of each species are

$$\frac{d[\text{M}]}{dt} = -k_1[\text{M}] \qquad (4)$$

$$\frac{d[\text{D}]}{dt} = k_1[\text{M}] - k_2[\text{D}] \qquad (5)$$

$$\frac{d[\text{Tr}]}{dt} = k_2[\text{D}] - k_3[\text{Tr}] \qquad (6)$$

$$\frac{d[\text{Tt}]}{dt} = k_3[\text{Tr}] \qquad (7)$$

Solving these differential equations yields solutions to describe time-dependent concentrations of each species:

$$[\text{M}] = [\text{M}]_0\, e^{-k_1 t} \qquad (8)$$

$$[\text{D}] = \frac{k_1[\text{M}]_0}{k_2 - k_1}(e^{-k_1 t} - e^{-k_2 t}) \qquad (9)$$

$$[\text{Tr}] = -\frac{k_1 k_2[\text{M}]_0}{(k_1 - k_2)(k_3 - k_1)}e^{-k_1 t} - \frac{k_1 k_2[\text{M}]_0}{(k_1 - k_2)(k_2 - k_3)}e^{-k_2 t} - \frac{k_1 k_2[\text{M}]_0}{(k_2 - k_3)(k_3 - k_1)}e^{-k_3 t} \qquad (10)$$

$$[\text{Tt}] = [\text{M}]_0 + \frac{k_2 k_3[\text{M}]_0}{(k_1 - k_2)(k_3 - k_1)}e^{-k_1 t} + \frac{k_1 k_3[\text{M}]_0}{(k_1 - k_2)(k_2 - k_3)}e^{-k_2 t} + \frac{k_1 k_2[\text{M}]_0}{(k_2 - k_3)(k_3 - k_1)}e^{-k_3 t} \qquad (11)$$

in which initial I-PNP monomer concentration, $[\text{M}]_0$, is 150, the number of particles analyzed here. By fitting kinetic data using these equations, the rate constant values of k_1, k_2 and k_3 were evaluated.

3. SUPPORTING REFERENCES

(43) Toshina-Ishii, C.; Boxer, S. G. *Langmuir* **2006**, *22*, 2384.

(44) Lee, G. M.; Ishihara, A.; Jacobson, K. A. *Proc. Natl Acad. Sci. U.S.A.* **1991**, *88*, 6274.

4. SUPPORTING MOVIES GUIDE

We provide six supporting movies as follows:

● Supporting movie S1:

The dark-field microscopy measurement of 80-nm gold nanoparticles dispersed in solution. Gold nanoparticles show three-dimensional random diffusion behaviours in solution state, and they are repetitively focused in and out. The movie is played in real time.

● Supporting movie S2:

Highly mobile gold nanoparticle probes that are tethered to a supported lipid bilayer.

The gold nanoparticle probes with a biotin valency of 1 were tethered to a supported lipid bilayer by streptavidin-biotin interaction. Most gold nanoparticle probes are highly mobile and show uniform scattering intensity and green color under the dark-field microscope. The movie is played in real time.

●Supporting movie S3:

Mobile and Immobile gold nanoparticle probes on the supported lipid bilayer. The movie is played in real time.

● Supporting movie S4:

Target DNA hybridization-induced single nanoparticle cluster formation on a supported lipid bilayer.

The mobile plasmonic probes are being assembled on immobile plasmonic probe site by target DNA hybridization. The stepwise increases of the scattering intensity and color change are observed in every monomer addition step. The movie is played in real time. The image scale is same with Figure 3b.

● Supporting movie S5:

Cluster growths from mobile nanoparticle pairs.

The cluster growth via the combination of monomeric PNP attachment and coalescence between nanoparticle clusters in a mobile plasmonic nanoparticle-modified SLB. DNA sequences on mobile nanoparticles can be hybridized to each other in this case. The movie is played in real time. The image scale is same with Supporting Fig. S6.

● Supporting movie S6:

Simultaneous cluster growths on the multiple immobile plasmonic nanoparticle sites.

Nanoparticle clusters with various clustering degrees are being formed simultaneously in the presence of target DNA sequence. Image vibration and nanoparticle flows in the left in the earlier time of the movie are owing to the target DNA injection. The movie is played with 5× speed. The image scale is same with the right image in Figure 4a.